

Real-time Adversarial Perturbations against Deep Reinforcement Learning Policies: Attacks and Defenses

Buse G. A. Tekgul

Aalto University
Espoo, Finland

buse.atlitekgul@aalto.fi

Samuel Marchal

F-Secure Corporation & Aalto University
Espoo, Finland

samuel.marchal@aalto.fi

Shelly Wang

University of Waterloo
Waterloo, Canada

shelly.wang@uwaterloo.ca

N. Asokan

University of Waterloo & Aalto University
Waterloo, Canada

asokan@acm.org

ABSTRACT

Recent work has shown that deep reinforcement learning (DRL) policies are vulnerable to adversarial perturbations. Adversaries can mislead policies of DRL agents by perturbing the state of the environment observed by the agents. Existing attacks are feasible in principle but face challenges in practice, for example by being too slow to fool DRL policies in real time. We show that using the Universal Adversarial Perturbation (UAP) method to compute perturbations, independent of the individual inputs to which they are applied to, can fool DRL policies effectively and in *real time*. We describe three such attack variants. Via an extensive evaluation using three Atari 2600 games, we show that our attacks are effective, as they fully degrade the performance of three different DRL agents (up to 100%, even when the l_∞ bound on the perturbation is as small as 0.01). It is faster compared to the response time (0.6ms on average) of different DRL policies, and considerably faster than prior attacks using adversarial perturbations (1.8ms on average). We also show that our attack technique is efficient, incurring an online computational cost of 0.027ms on average. Using two further tasks involving robotic movement, we confirm that our results generalize to more complex DRL tasks. Furthermore, we demonstrate that the effectiveness of known defenses diminishes against universal perturbations. We propose an effective technique that detects all known adversarial perturbations against DRL policies, including all the universal perturbations presented in this paper.

KEYWORDS

deep reinforcement learning, adversarial examples, neural networks

1 INTRODUCTION

Machine learning models are vulnerable to *adversarial examples*: maliciously crafted inputs generated by adding small perturbations to the original input in order to force a model into generating wrong predictions [9, 31]. Prior work [11, 14, 16, 37] has shown that adversarial examples can also fool deep reinforcement learning (DRL) agents that use deep neural networks (DNNs) to approximate their *policy* (the decision-making strategy). If this vulnerability is exploited in safety-critical DRL applications such as robotic surgery and autonomous driving, the impact can be disastrous.

A DRL agent can partially or fully observe the *state* of the environment by capturing complex, high-dimensional observations.

For example, a DRL agent playing an Atari 2600 game observes pixels from each image frame of the game to construct states by combining a number of observations. DRL agents use the current state as an input to their policy which outputs a suitable action for that state. Consequently, adversaries can modify the environment to mislead the agent's sequential decision-making process. Various state-of-the-art attack methods assume *white-box* knowledge, where adversaries have access to the parameters of the agent's policy model and the reinforcement learning algorithm. In *untargeted* attacks, the adversary's goal is to fool the agent's policy so that the agent becomes useless. The agent is useless when it 1) cannot complete its task or 2) finishes its task with unacceptably poor performance. Prior work has shown that adversaries with white-box knowledge can successfully destroy an agent's performance using one-step gradient-based approaches [9], optimization-based methods [6], or adversarial saliency maps [25]. Previous work has also proposed different attack strategies where the adversary generates the perturbation for 1) each state [2, 11], 2) *critical states* where the agent prefers one action with high confidence [14, 16, 29], or 3) periodically, at every N^{th} state [14].

Although prior white-box attacks using adversarial perturbations are effective in principle, they are not realistic in practice. First, some attack strategies [11, 16] are based on computing the perturbation using back-propagation or solving an optimization problem. This is computationally expensive even if it is done for every N^{th} state. DRL agents need to respond new states very quickly in order to carry out the task effectively. Attacks that take longer than the average time between the agent response and the sampling of the next state are too slow to be implemented in real-time. Second, in realistic scenarios, the adversary cannot have full control over the environment. However, iterative attacks [16, 37] require querying agents with multiple perturbed versions of the current state and resetting the environment in order to find the optimal perturbation. Therefore, iterative attacks cannot be applied in real-life scenarios such as autonomous agents interacting with a dynamic environment. Finally, the aforementioned state-the-art attacks require seeing all observations to generate and apply perturbations to the state containing multiple observations. However, the agent can store clean observations that are part of the current state in its memory before the adversary can generate perturbations that need to be applied to *all of those observations*. In order to overcome these challenges, Xiao *et al.* [37] proposed a new attack strategy

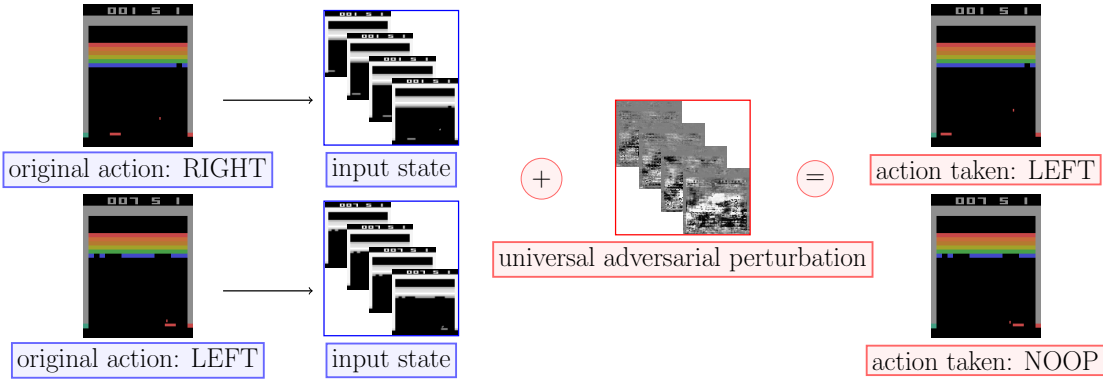


Figure 1: In the Breakout game, when a universal adversarial perturbation is added into different states, it causes the policy of a victim DQN agent to take sub-optimal actions instead of optimal actions, i.e., fail to catch the ball and lose the game.

by producing a single, *universal perturbation* during the task. This method generates perturbations that are independent of the input state and can be mounted in real time. However, it assumes that the task can be suspended (freezing the agent and the environment) to allow time generating the perturbation *online* for each start. (in other words, each start requires a different universal perturbation). In many settings, this is not a realistic assumption.

Contributions. We propose an effective, *real-time* attack strategy to fool DRL policies by computing a state-agnostic, universal perturbations *offline*. Once this perturbation is generated, it can be added into any state to force the victim agent into choosing sub-optimal actions (Figure 1). Similar to previous work [37], we focus on untargeted attacks in a white-box setting. Our contributions are:

- (1) We design two new real-time white-box attacks, UAP-S and UAP-O, using Universal Adversarial Perturbation (UAP) [21] to generate state-agnostic adversarial examples. We also design a third real-time attack, OSFW(U), by extending Xiao *et al.*'s [37] attack so that it generates a universal perturbation once, applicable to *any subsequent episode* (Section 3). An empirical evaluation of these three attacks using three different reinforcement learning algorithms playing three different Atari 2600 games (Breakout, Freeway, and Pong) demonstrates that our attacks are comparable to prior work in their effectiveness (100% drop in return), while being *significantly faster* (0.027 ms on average, compared to 1.8 ms) and *less visible* than prior adversarial perturbations [11, 37] (Section 4.2). Using two additional tasks involving the MuJoCo robotics simulator [33], which requires continuous control, we show that our results generalize to more complex DRL agents (Section 4.3).
- (2) We demonstrate the limitations of prior defenses. We show that agents trained with the state-of-the-art robust policy regularization technique [39] exhibit reduced effectiveness against adversarial perturbations at higher perturbation bounds (> 0.05). In some tasks (Pong), universal adversarial perturbations completely destroy the agent performance (Table 2). Visual Foresight [17], which can completely restore an agent's

performance in the presence of prior adversarial perturbations [11], fails to do so when faced with universal perturbations (Section 5.2).

- (3) We propose an efficient method, AD³, to detect adversarial perturbations. AD³ can be combined with other defenses to provide stronger resistance for DRL agents against untargeted adversarial perturbations (Section 5.3).

2 BACKGROUND AND RELATED WORK

2.1 Deep Reinforcement Learning

2.1.1 Reinforcement learning. Reinforcement learning involves settings where an agent continuously interacts with a non-stationary environment to decide which action to take in response to a given state. At time step t , the environment is characterized by its state $s \in \mathcal{S}$ consisting of N past observations o pre-processed by some function f_{pre} , i.e., $s = \{f_{pre}(o_{t-N+1}), \dots, f_{pre}(o_t)\}$. At each s , the agent takes an action $a \in \mathcal{A}$ which moves the environment to the next $s' \in \mathcal{S}$ and yields a reward r from the environment. The agent uses this information to optimize its policy π , a probability distribution that maps states into actions [30]. During training, the agent improves the estimate of a value function $V(s)$ or an action-value function $Q(s, a)$. $V(s)$ measures how valuable it is to be in a state s by calculating the *expected discounted return*: the discounted cumulative sum of future rewards while following a specific π . Similarly, $Q(s, a)$ estimates the value of taking action a in the current s when following π . During evaluation, the optimized π is used for decision making, and the *performance* of the agent is measured by the return. In this work, we focus on *episodic* [4] and *finite-horizon* [32] tasks. In episodic tasks such as Atari games, each episode ends with a terminal state (e.g., winning/losing a game, arriving at a goal state). In this case, the return for one episode is computed by the total score in single-player games (e.g., Breakout, Freeway) or the relative score when it is played against a computer (e.g., Pong). Finite-horizon tasks includes continuous control, where (e.g., Humanoid, Hopper) the return is measured for a fixed length of the episode.

2.1.2 DNN. DNNs are parameterized functions $f(\mathbf{x}, \theta)$ consisting of neural network layers. For an input $\mathbf{x} \in \mathbb{R}^n$ with n features, the

parameter vector θ is optimized by training the DNN over a labeled training set. $f(\mathbf{x}, \theta)$ outputs a vector $\mathbf{y} \in \mathbb{R}^m$ with m different classes. In classification problems, one can find the predicted class as $\hat{f}(\mathbf{x}) = \operatorname{argmax}_m f(\mathbf{x}, \theta)$. For simplicity, we will use $f(\mathbf{x})$ to denote $f(\mathbf{x}, \theta)$.

2.1.3 DRL. DNNs are useful for approximating π when \mathcal{S} or \mathcal{A} is too large, or largely unexplored. Deep Q Networks (DQN) is one of the well-known *value-based* DRL algorithms [20] that uses DNNs to approximate $Q(\mathbf{s}, a)$. During training, the DQN aims to find the optimal $Q(\mathbf{s}, a)$ by updating the estimate of $Q(\mathbf{s}, a)$ repeatedly with actions that maximize $Q(\mathbf{s}, a)$ in each step. Therefore, the optimal π is defined implicitly by using the optimal $Q(\mathbf{s}, a)$. Despite its effectiveness, DQN cannot be used in continuous control tasks, where a is a real-valued vector sampled from a range, instead of a finite set. Continuous control tasks require different *policy-based* DRL algorithms [19, 28]. They use two different DNNs that usually share a number of lower layers, to approximate both π and $V(\mathbf{s})$ (or $Q(\mathbf{s}, a)$ depending on the algorithm), and update π directly. For example, in *actor-critic* methods (A2C) [19], the critic estimates $V(\mathbf{s})$ or $Q(\mathbf{s}, a)$ for the current π and the actor updates the parameter vector θ of π by using the *advantage*. Advantage refers to the critic's evaluation of the action decision using the estimated $V(\mathbf{s})$ or $Q(\mathbf{s}, a)$, while the actor is following the current π . Proximal Policy Optimization (PPO) [28] is an on-policy variant of A2C. PPO updates the current π by ensuring that the updated π is close to the old one.

2.2 Adversarial Examples

An adversarial example \mathbf{x}^* against a classification model $f(\mathbf{x})$ is a deliberately modified version of an input \mathbf{x} such that \mathbf{x} and \mathbf{x}^* are similar, but \mathbf{x}^* is misclassified by f , i.e., $\hat{f}(\mathbf{x}) \neq \hat{f}(\mathbf{x}^*)$. An untargeted adversarial example is found by solving

$$\begin{aligned} & \operatorname{argmax}_{\mathbf{x}^*} \ell(f(\mathbf{x}^*), \hat{f}(\mathbf{x})) \\ & \text{s.t.: } \|\mathbf{x}^* - \mathbf{x}\|_p = \|\mathbf{r}\|_p \leq \epsilon, \end{aligned} \quad (1)$$

where ϵ is the l_p perturbation constraint and ℓ is the loss between $f(\mathbf{x}^*)$ and the predicted label $\hat{f}(\mathbf{x})$. In this work, we assume the l_∞ constraint (i.e., any element in the perturbation must not exceed a specified threshold ϵ) as in the state-of-the-art Fast Gradient Sign Method (FGSM) [9]. FGSM calculates \mathbf{r} by

$$\mathbf{r} = \epsilon \cdot \operatorname{sign}(\nabla_{\mathbf{x}} \ell(f(\mathbf{x}), \hat{f}(\mathbf{x}))). \quad (2)$$

Usually, adversarial examples are computed for each \mathbf{x} . An alternative is to generate input-agnostic *universal perturbations*. For instance, Moosavi *et al.* propose *Universal Adversarial Perturbation* (UAP) [21] that searches for a sufficiently small \mathbf{r} that can be added to *arbitrary* inputs to yield adversarial examples against f . UAP iteratively computes a unique \mathbf{r} that fools the classifier for almost all inputs \mathbf{x} belonging to a training set $\mathcal{D}_{\text{train}}$. UAP utilizes DeepFool [22] to update \mathbf{r} at each iteration. In addition to the l_∞ constraint, UAP should achieve a desired *fooling rate* δ : the proportion of successful adversarial examples against f with respect to the total number of perturbed samples $|\mathcal{D}_{\text{train}}|$ in $\mathcal{D}_{\text{train}}$.

Following the first work [21] introducing UAP, many different strategies [7, 10, 23, 24] have been proposed to generate UAPs to fool image classifiers. Hayes *et al.* [10] and Mopuri *et al.* [24] use

generative models that can learn the distribution of UAPs and obtain different UAPs for image datasets. Mopuri *et al.* [23] introduce the Fast Feature Fool algorithm to fool features in different layers without the need of the training dataset. Co *et al.* [7] design black-box, untargeted UAPs using procedural noise functions.

2.3 Adversarial Examples against DRL Policies

In discrete action spaces, where agents have finite actions, adversarial examples against a DRL policy is found by modifying Equation 1: \mathbf{x} is changed into \mathbf{s} at time t , and f is replaced with $Q(\mathbf{s}, a)$. Given \mathbf{s} and $Q(\mathbf{s}, a)$, $\hat{Q}(\mathbf{s})$ refers to the action decision. We also denote $Q(\mathbf{s}, a_m)$ as the state-action value of m^{th} action at \mathbf{s} . In this setup, adversarial examples are computed to decrease $Q(\mathbf{s}, a)$ for the optimal action at \mathbf{s} , resulting in a sub-optimal decision.

Since Huang *et al.* [11] showed the vulnerability of DRL policies against adversarial perturbations, several untargeted attack methods [2, 14, 16, 29, 37] have been proposed for manipulating the environment. Recent work [1, 6, 12, 16, 35] has also developed targeted attacks, where the adversary's goal is to lure the victim policy into a specific state or to force the victim policy into following a specific path. Most of these methods implement well-known adversarial example generation methods such as FGSM [11, 14], JSMA [2] and Carlini&Wagner [16]. Therefore, even though they effectively decrease the return of the agent, these methods cannot be implemented in real-time and have a temporal dependency: they need to compute a different \mathbf{r} for every \mathbf{s} . Similar to our work and Xiao *et al.* [37], Hussinet *et al.* [12] designed targeted attacks that use different universal perturbations for each action to force the victim policy into following the adversary's policy. The universal perturbation from Xiao *et al.* ("obs-seq-fgsm-wb", OSFW) is computed by applying FGSM to averaged gradients over k states to compute a single \mathbf{r} , and adding it to the remaining states in the current episode. OSFW has limitations such as the need to compute \mathbf{r} for every new episode. Moreover, it has to freeze the task to calculate \mathbf{r} using the victim agent, and its performance depends on the particular agent-environment interaction for each episode.

In addition to white-box attacks, multiple black-box attack methods based on finite-difference methods [37], and proxy methods approximating the victim policy [13, 41] were proposed, but they cannot be mounted in real time, since they require querying the agent multiple times.

Recent work [8, 36] shows that adversaries can fool DRL policies in multi-agent, competitive games by training an adversarial policy for the opponent agent that exploits vulnerabilities of the victim agent. These attacks rely on creating natural observations with adversarial effects, instead of manipulating the environment by adding adversarial perturbations. In this paper, we focus on single-player games, where adversaries can only modify the environment in order to fool DRL policies.

3 STATE- AND OBSERVATION-AGNOSTIC PERTURBATIONS

We first define our adversary model and then formally present two new attacks—state-agnostic UAP (UAP-S) and observation-agnostic UAP (UAP-O)—and an improved variant, OSFW(U), of a prior attack.

3.1 Adversary Model

The goal of the adversary Adv is to degrade the performance of the victim DRL agent v by adding perturbations \mathbf{r} to state \mathbf{s} observed by v . Adv is successful when the attack:

- (1) is *effective*, i.e., limits v to a low return,
- (2) is *efficient*, i.e., can be realized in real-time, and
- (3) *evades* known detection mechanisms.

Adv has a white-box access to v ; therefore, it knows v 's action value function Q_v , or the policy π_v and the value function V_v , depending on the DRL algorithm used by v . However, Adv is constrained to using \mathbf{r} with a small norm to evade possible detection, either by specific anomaly detection mechanisms or via human observation. In addition, we assume that Adv cannot reset the environment or return to an earlier state. In other words, we rule out trivial attacks (e.g., swapping one video frame with another or changing observations with random noise) as ineffective because they can be easily detected.

3.2 Attack Design

3.2.1 Training data collection. Adv collects a training set \mathcal{D}_{train} by monitoring v 's interaction with the environment for one episode, and saving each \mathbf{s} into \mathcal{D}_{train} . Simultaneously, Adv clones Q_v or V_v into a *proxy agent*, adv . Specifically, in value-based methods (e.g., DQN), Adv copies weights of Q_v into Q_{adv} . In policy based methods, (e.g., A2C, PPO), Adv copies weights of the critic network into V_{adv} . In the latter case, Adv can obtain $Q_{adv}(\mathbf{s}, a)$ by calculating $V_{adv}(\mathbf{s})$ for each discrete action a in \mathcal{A} .

3.2.2 Data sanitization. Adv sanitizes \mathcal{D}_{train} by choosing only the *critical states*. Following [16], we define critical states as those that can have a significant influence on the course of the episode. We identify critical states using the relative action preference function

$$\begin{aligned} \text{Var}_{a \in \mathcal{A}} [\text{Softmax}(Q_{adv}(\mathbf{s}, a))] &\geq \beta \\ \beta = \frac{1}{|\mathcal{D}_{train}|} \sum_{s \in \mathcal{D}_{train}} \text{Var}_{a \in \mathcal{A}} [\text{Softmax}(Q_{adv}(\mathbf{s}, a))] \end{aligned} \quad (3)$$

modified from [16], where Var is the variance of normalized $Q_{adv}(\mathbf{s}, a)$ values computed for $\forall a \in \mathcal{A}$. This ensures that both UAP-S and UAP-O are optimized to fool Q_v in critical states, and achieves the first attack criterion.

3.2.3 Computation of perturbation. For both UAP-S and UAP-O, we assume that $\mathbf{s} \in \mathcal{D}_{train}$ and $\mathcal{D}_{train} \subset \mathcal{S}$. Adv searches for an optimal \mathbf{r} that satisfies the constraints in Equation 1 while achieving a high fooling rate δ on \mathcal{D}_{train} . For implementing UAP-S and UAP-O, we modify the Universal Adversarial Perturbation method in [21] (see Section 2.2) that uses DeepFool [22] to solve Equation 1. The goal of both UAP-S and UAP-O is to find a sufficiently small \mathbf{r} such that $\hat{Q}(\mathbf{s} + \mathbf{r}) \neq \hat{Q}(\mathbf{s})$, leading v to choose sub-optimal actions. Algorithm 1 summarizes the method to generate UAP-S and UAP-O.

In lines 5-6 of Algorithm 1, DeepFool computes the additional $\Delta\mathbf{r}$ by iteratively updating the perturbed $\mathbf{s}_i^* = \mathbf{s} + \mathbf{r} + \Delta\mathbf{r}_i$ until \hat{Q}_{adv} outputs a wrong action (see Algorithm 2 in [22]). At each iteration i , DeepFool finds the closest hyperplane $\hat{l}(\mathbf{s}_i^*)$ and $\Delta\mathbf{r}_i$ that projects \mathbf{s}_i^* on the hyperplane. It re-computes $\Delta\mathbf{r}_i$ as

Algorithm 1: Computation of UAP-S and UAP-O

```

input : sanitized  $\mathcal{D}_{train}$ ,  $Q_{adv}$ , desired fooling rate  $\delta_{th}$ ,  

       max. number of iterations  $it_{max}$ , pert. constraint  $\epsilon$ 
output: universal  $\mathbf{r}$ 
1 Initialize  $\mathbf{r} \leftarrow 0$ ,  $it \leftarrow 0$ ;
2 while  $\delta < \delta_{max}$  and  $it < it_{max}$  do
3   for  $\mathbf{s} \in \mathcal{D}_{train}$  do
4     if  $\hat{Q}(\mathbf{s} + \mathbf{r}) \neq \hat{Q}(\mathbf{s})$  then
5       Find the extra, minimal  $\Delta\mathbf{r}$ :
6        $\Delta\mathbf{r} \leftarrow \text{argmin}_{\Delta\mathbf{r}} \|\Delta\mathbf{r}\|_2$  s.t.  $\hat{Q}(\mathbf{s} + \mathbf{r} + \Delta\mathbf{r}) \neq \hat{Q}(\mathbf{s})$ ;
7        $\mathbf{r} \leftarrow \text{sign}(\min(\text{abs}(\mathbf{r} + \Delta\mathbf{r}), \epsilon))$ ;
8   Calculate  $\delta$  with updated  $\mathbf{r}$  on  $\mathcal{D}_{train}$ ;
9    $it \leftarrow (it + 1)$ ;

```

$$\begin{aligned} Q'(\mathbf{s}_i^*, a_i) &\leftarrow Q_{adv}(\mathbf{s}_i^*, a_i) - Q_{adv}(\mathbf{s}_i^*, a_m), \\ \mathbf{w}'_i &\leftarrow \nabla Q_{adv}(\mathbf{s}_i^*, a_i) - \nabla Q_{adv}(\mathbf{s}_i^*, a_m), \\ \Delta\mathbf{r}_i &\leftarrow \frac{|Q'(\mathbf{s}_i^*, a_i)|}{\|\mathbf{w}'_i\|^2} \mathbf{w}'_i \end{aligned} \quad (4)$$

where ∇ is the gradient of Q_{adv} w.r.t \mathbf{s}_i and $Q_{adv}(\mathbf{s}_i^*, a_m)$ is the value of the m -th action that was chosen for the state $\mathbf{s} + \mathbf{r}$.

In UAP-S, there is a different perturbation for each observation o_j in \mathbf{s} , i.e., $\mathbf{r} = \{r_{t-N+1}, \dots, r_t\}$, $r_j \neq r_k$, $\forall j, k \in \{t-N+1, \dots, t\}$, $j \neq k$. In contrast, for UAP-O, the same perturbation is applied to all observations in \mathbf{s} . Therefore, it can be considered as an observation-agnostic, completely universal attack. UAP-O aims to find a modified version $\tilde{\mathbf{r}}$ of \mathbf{r} by solving

$$\begin{aligned} \min(\|\mathbf{r} - \tilde{\mathbf{r}}\|_2^2) \\ \text{s.t.: } \tilde{r}_j = \tilde{r}_k, \forall j, k \in \{t - N + 1, \dots, t\} \text{ and } \|\tilde{\mathbf{r}}\|_\infty \leq \epsilon. \end{aligned} \quad (5)$$

To compute UAP-O, we modify lines 5 and 6 of Algorithm 1 that finds $\Delta\mathbf{r}$. The closest $\Delta\tilde{\mathbf{r}}_i$ to $\Delta\mathbf{r}_i$ satisfying the conditions in Equation 5 is found by averaging \mathbf{w}'_i over observations:

$$\Delta\tilde{\mathbf{r}}_i \leftarrow \frac{|Q'(\mathbf{s}_i^*, a_i)|}{N \|\mathbf{w}'_i\|^2} \sum_{k=(t-N+1)}^t \mathbf{w}'_{i_k}, \forall j \in \{t - N + 1, \dots, t\}. \quad (6)$$

In UAP-O, DeepFool returns $\Delta\tilde{\mathbf{r}}_i = \Delta\tilde{\mathbf{r}}_j$ as the optimal, extra perturbation. UAP-O adds the same perturbation \tilde{r}_j to every observation o_j in \mathbf{s} . If the input state consists of only one observation, then UAP-S will simply reduce to UAP-O. The proof for Equation 6 can be found in Appendix A.

3.2.4 Extending OSFW to OSFW(U). As explained in Section 2.3, OSFW calculates \mathbf{r} by averaging gradients of Q_v using first k states in an episode, and then adds \mathbf{r} into remaining states. This requires 1) generating a different \mathbf{r} for each episode, and 2) suspending the task and v to perform backward propagation. Moreover, the effectiveness of OSFW varies when v behaves differently in individual episodes. We extend OSFW to a completely universal adversarial

Algorithm 2: Computation of UAP in continuous control

```
input :sanitized  $\mathcal{D}_{train}$ ,  $V_{adv}$ , hyper-parameter  $\alpha$ 
       max. number of iterations  $it_{max}$ , pert. constraint  $\epsilon$ 
output:universal  $r$ 
1 Initialize  $r \leftarrow 0$ ,  $it \leftarrow 0$ ;
2 while  $\delta < \delta_{max}$  and  $it < it_{max}$  do
3   for  $s \in \mathcal{D}_{train}$  do
4     if  $V_{adv}(s + r) + \alpha < V_{adv}(s)$  then
5       Find the extra, minimal  $\Delta r$ :
6        $\Delta r \leftarrow \operatorname{argmin}_{\Delta r} \|\Delta r\|_2$ 
7       s.t.  $V_{adv}(s + r + \Delta r) + \alpha < V_{adv}(s)$ ;
8        $r \leftarrow \operatorname{sign}(\min(\operatorname{abs}(r + \Delta r), \epsilon))$ ;
9   Calculate  $\delta$  with updated  $r$  on  $\mathcal{D}_{train}$ ;
10   $it \leftarrow (it + 1)$ ;
```

perturbation by using the proxy agent’s DNN, and calculate averaged gradients with first k samples from the same, un-sanitized \mathcal{D}_{train} . The formula for calculating r in OSFW(U) is

$$r = \epsilon \cdot \operatorname{sign}\left(\frac{1}{k} \sum_{i=0}^{i < k} \nabla_{s_i}(-\log(Q_{adv}(s_i, \hat{a})))\right); \quad (7)$$

where \hat{a} denotes the chosen action and $s_i \in \mathcal{D}_{train}$.

3.3 Attacks in Continuous Control Settings

In continuous control tasks, the optimal action is a real-valued array that is selected from a range. These tasks have complex environments involving physical systems control such as Humanoid robots with multi-joint dynamics [33]. In continuous control, unlike discrete tasks, there is no available $Q(s, a)$ for generating perturbations and decreasing the value of the optimal action. Nevertheless, Adv can find a perturbed state $s + r$ having the worst value so that the action chosen by the policy of v , π_v , will be a bad decision [39]. In continuous control, FGSM, OSFW and OSFW(U) can be simply modified by changing Q_{adv} with V_{adv} . However, in Algorithm 1, lines from 4 and 6 needs to be adjusted to handle these tasks. Adv can only use the copied network parameters of V_{adv} to find r . The corrected computation for UAP-S and UAP-O is given in Algorithm 2. In each iteration it , Δr is found by solving the optimization problem (lines 5 and 6).

4 ATTACK EVALUATION

We compared the effectiveness of our attacks (UAP-S, UAP-O and OSFW(U)) with prior attacks (FGSM and OSFW) on discrete tasks using three Atari 2600 games (Pong, Breakout, Freeway) in the Arcade Learning Environment [4]. We further extended our experimental setup with the MuJoCo robotics simulator [33] and compared these attacks in continuous control tasks.

4.1 Experimental Setup

To provide an extensive evaluation, for every Atari game, we trained three agents each using a different DRL algorithm: value-based DQN [20], policy-based PPO [28] and actor-critic method A2C [19].

We used the same DNN architecture proposed in [20] for approximating Q_v in DQN and V_v in other algorithms. To facilitate comparison, we used the same setup to implement all DRL policies as well as the different attacks: PyTorch (version 1.2.0), NumPy (version 1.18.1), Gym (a toolkit for developing reinforcement learning algorithms, version 0.15.7) and MuJoCo 1.5 libraries. All experiments were done on a computer with 2x12 core Intel(R) Xeon(R) CPUs (32GB RAM) and NVIDIA Quadro P5000 with 16GB memory.

Our implementations of DQN, PPO and A2C are based on OpenAI baselines¹, and our implementations achieve similar returns as in OpenAI Baselines. For pre-processing, we converted each RGB frame to gray-scale, re-sized those from 210×160 to 84×84 , and normalized the pixel range from $[0, 255]$ to $[0, 1]$. We used the frame-skipping technique, where the victim v constructs s at every N^{th} observation, then selects an action and repeats it until the next state s' . We set $N = 4$ so the input state size is $4 \times 84 \times 84$. We also kept the frame rate of each game as 60 Hz; thus, the time interval between consecutive states is $4/60 = 0.067$ seconds.

We implemented UAP-S, UAP-O and OSFW(U) by setting the desired δ_{max} to 95%, so that both UAP-S and UAP-O stop searching for another r when $\delta \geq 95\%$. As baselines, we used random noise addition, FGSM [11], and OSFW [37]. We measured attack effectiveness when ϵ is between 0 and 0.01. We reported the average return over 10 episodes and run each episode with a different seed during training and evaluation.

4.2 Attack Performance

4.2.1 Performance degradation. Figure 2 compares UAP-S, UAP-O, and OSFW(U) with two baseline attacks and random noise addition. As can be seen from the figure, random noise addition cannot cause a significant drop in v ’s performance, and FGSM is the most effective attack reducing the return up to 100% even with a very small ϵ value. UAP-S is the second most effective attack in almost every setup, reducing the return by more than 50% in all experiments when $\epsilon \geq 0.004$. Additionally, all adversarial perturbations completely destroy agents’ performance at $\epsilon = 0.01$, except the PPO agent playing Freeway. The effectiveness of UAP-O, OSFW, and OSFW(U) are comparable across all setups. We also observe that the effectiveness of OSFW fluctuates heavily (A2C agent playing Breakout) or has high variance (PPO agent playing Freeway). This phenomenon is the result of v ’s different behaviours in individual episodes (A2C agent playing Breakout), and OSFW’s inability to collect enough knowledge (PPO agent playing Freeway) in order to generalize r to the rest of the episode.

4.2.2 Timing comparison. Table 1 presents the computational cost for generating r (at $\epsilon = 0.01$) and agents’ response times (the time spent for feeding s forward through π_v or Q_v). Table 1 confirms that the online costs of OSFW and FGSM are higher than all other attacks and, more importantly, v ’s response time and the time interval between consecutive states. Thus, these attacks cannot be applied in real-time. UAP-S and UAP-O have a higher offline cost than OSFW(U), but the offline generation of r does not interfere with the task, since UAP-S and UAP-O do not require interrupting or pausing v . The online cost of UAP-S, UAP-O and OSFW(U) is lower

¹<https://github.com/DLR-RM/rl-baselines3-zoo>

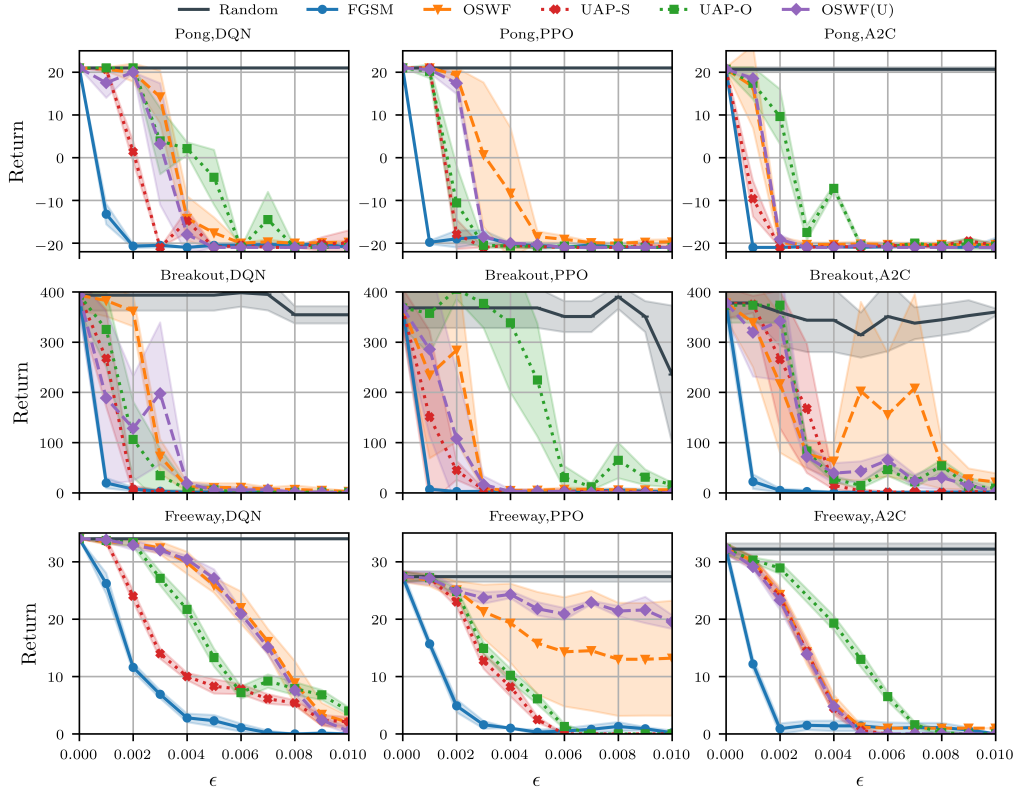


Figure 2: Comparison of attacks against three different policy networks (DQN, PPO, A2C) trained for three Atari games (Pong, Breakout, Freeway). The graph shows how the return (averaged over 10 games) changes with different ϵ values for six different attack strategies.

Experiment	Attack method	Offline cost \pm std (seconds)	Online cost \pm std (seconds)
Pong, DQN, Agent's response time: $4 \times 10^{-4} \pm 10^{-6}$ sec	FGSM	-	$13 \times 10^{-4} \pm 10^{-5}$
	OSFW	-	5.3 ± 0.1
	UAP-S	36.4 ± 21.1	$2.7 \times 10^{-5} \pm 10^{-6}$
	UAP-O	138.3 ± 25.1	$2.7 \times 10^{-5} \pm 10^{-6}$
	OSFW(U)	5.3 ± 0.1	$2.7 \times 10^{-5} (\pm 10^{-6})$
	FGSM	-	$21 \times 10^{-4} \pm 10^{-5}$
Pong, PPO, Agent's response time: $9.3 \times 10^{-4} \pm 10^{-5}$ sec	OSFW	-	7.02 ± 0.6
	UAP-S	41.9 ± 16.7	$2.7 \times 10^{-5} \pm 10^{-6}$
	UAP-O	138.3 ± 25.1	$2.7 \times 10^{-5} \pm 10^{-6}$
	OSFW(U)	7.02 ± 0.6	$2.7 \times 10^{-5} \pm 10^{-6}$
Pong, A2C, Agent's response time: $9.3 \times 10^{-4} \pm 10^{-5}$ sec	FGSM	-	$21 \times 10^{-4} \pm 10^{-5}$
	OSFW	-	7.2 ± 1.1
	UAP-S	11.4 ± 4.3	$2.7 \times 10^{-5} \pm 10^{-6}$
	UAP-O	55.5 ± 29.3	$2.7 \times 10^{-5} \pm 10^{-6}$
	OSFW(U)	7.2 ± 1.1	$2.7 \times 10^{-5} \pm 10^{-6}$

Table 1: Offline and online comparison of attacks in terms of the time spent for the perturbation generation and mounting the attack during deployment. Victim agents are DQN, PPO, A2C trained for Pong and $\epsilon = 0.01$. Attacks that cannot be implemented in real-time are in highlighted in red.

than v 's response time and the time interval between consecutive states; therefore, they can be mounted in real-time.

4.2.3 Difference in perturbation sizes. We compared the maximum size of perturbation added into observations for different attacks. Figure 3 shows that the perturbation obtained via UAP-S and UAP-O are smaller than other adversarial perturbations for a given ϵ value. This is because UAP-S and UAP-O try to find a minimal perturbation that sends all $\mathbf{x} \in \mathcal{D}_{train}$ outside the decision boundary [21]. We conclude that UAP-S and UAP-O are likely to be less detectable based on perturbation sizes (e.g., via visual observation).

As shown in Table 2 summarizing the characteristics of all attacks implemented in the paper, FGSM and OSFW cannot be mounted in real-time and need pre-computation for each s or once in every episode. UAP-S, UAP-O and OSFW(U) are real-time attacks that do not require stopping the agent or the environment while adding the perturbation. UAP-S and OSFW(U) generate a perturbation \mathbf{r} that is independent from s , but the r_j for each observation $o_j \in s$ is different. On the other hand, UAP-O can be considered as both observation- and state-agnostic: it adds the same r_j to all observations in any s . UAP-O leads to an efficient and effective attack when $\epsilon \geq 0.006$, and it is the only attack that does not have

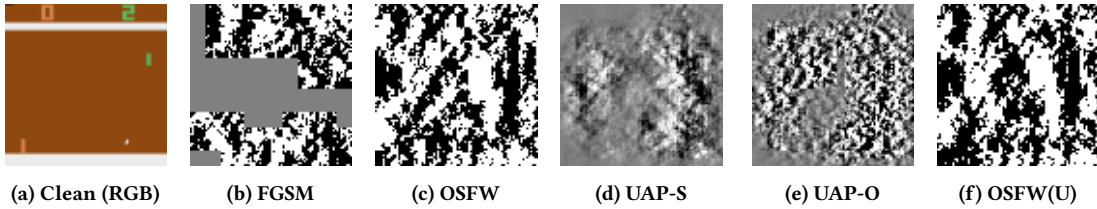


Figure 3: Comparison of perturbation size added into the same clean (RGB) observation in different attacks against the DQN agent playing Pong and $\epsilon = 0.01$. In perturbations, black pixels: -0.01 , white pixels: $+0.01$, gray pixels: 0.0 .

Attack Method	Real-time	Temporal dependency	Observation dependency
FGSM [11]	No	Dependent	Dependent
OSFW [37]	No	Dependent	Dependent
<u>UAP-S</u>	Yes	Independent	Dependent
<u>UAP-O</u>	Yes	Independent	Independent
<u>OSFW(U)</u>	Yes	Independent	Dependent

Table 2: Summary of five attacks based on the characteristics that makes an attack plausible in a real deployment scenario. New attacks proposed in this paper are highlighted in blue and underlined.

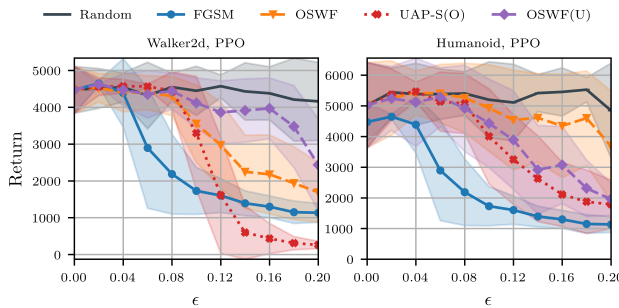


Figure 4: Comparison of attacks against PPO agents trained for Humanoid and Walker-2d tasks. The graph shows how the return (averaged over 50 games) changes with different ϵ values for five different attack strategies.

temporal and observational dependency. UAP-S is the best attack considering both effectiveness and efficiency.

In simple environments like Atari 2600 games, sequential states are not i.i.d. Moreover, Atari 2600 games are *controlled* environments, where future states are predictable and episodes do not deviate much from one another for the same task. OSFW and OSFW(U) leverage this non-i.i.d property. However, their effectiveness might decrease in uncontrolled environments and the physical world due to the uncertainty of the future states. In contrast, UAP-S is independent of the correlation between sequential states. To confirm our conjecture, we implemented OSFW(U) against VGG-16 image classifiers [40] pre-trained on ImageNet [27], where ImageNet can be viewed as a non i.i.d., uncontrolled environment. We measured that

Experiment	Attack method	Offline cost \pm std (seconds)	Online cost \pm std (seconds)
Walker2d, PPO, Agent's response time: $9.2 \times 10^{-5} \pm 10^{-6}$ sec	FGSM	-	$31 \times 10^{-5} \pm 10^{-5}$
	OSFW	-	0.02 ± 0.001
	UAP-S (O)	8.75 ± 0.024	$2.9 \times 10^{-5} \pm 10^{-6}$
	OSFW(U)	0.02 ± 0.001	$2.9 \times 10^{-5} \pm 10^{-6}$
Humanoid, PPO, Agent's response time: $9.6 \times 10^{-5} \pm 10^{-6}$ sec	FGSM	-	$35 \times 10^{-5} \pm 10^{-5}$
	OSFW	-	0.02 ± 0.001
	UAP-S (O)	35.86 ± 0.466	$2.4 \times 10^{-5} \pm 10^{-6}$
	OSFW(U)	0.02 ± 0.001	$2.4 \times 10^{-5} \pm 10^{-6}$

Table 3: Offline and online comparison of attacks in terms of the time spent for the perturbation generation and mounting the attack during deployment. Victim agents are PPO trained for Walker2d and Humanoid at $\epsilon = 0.02$. Attacks that cannot be implemented in real-time are highlighted in red.

OSFW(U) achieves a fooling rate of up to 30% on the ImageNet validation set with $\epsilon = 10$, while UAP-S has a fooling rate of 78% [21], where the l_∞ norm of an image in the validation set is around 250. Therefore, we conclude that UAP-S can mislead DRL policies more than OSFW(U) in complex, uncontrolled environments.

4.3 Attack Performance in Continuous Control

We now consider continuous control tasks to see whether our observations regarding the effectiveness of universal adversarial perturbations generalize beyond discrete tasks. As we explained in Section 2, only policy-based DRL methods are suitable in continuous control tasks. We focus on PPO, since it is more recent than A2C, and is considered to be the state-of-the-art reinforcement learning algorithm [28]. For v , we used previously trained PPO agents [39] for two different MuJoCo environments: Walker2d and Humanoid². We used the experimental setup given by authors in their GitHub repository to test PPO agents and compared our attacks with baseline attacks as well as random noise addition. In our experiments, PPO agents show similar performance as the ones reported in the original paper [39]. We implemented UAP-S by copying the parameters of V_v into V_{adv} , and set $\delta_{max} = 95\%$. We should note that FGSM, OSFW and OSFW(U) also use V_v to minimize the value in a perturbed state, instead of Q_v , which is not available in continuous control. Additionally, in both tasks, s contains only one observation, thus reducing UAP-S to UAP-O.

Figure 4 shows the attack effectiveness when ϵ is between 0.0 and 0.2. FGSM is the most effective attack in Humanoid, while UAP-S decreases the return more than FGSM in Walker2d when

²Agents are downloaded from https://github.com/huanzhang12/SA_PPO

$\epsilon \geq 0.12$. Overall, all attacks behave similarly in both discrete and continuous action spaces. Therefore, our conclusions regarding the effectiveness of universal adversarial perturbations generalize to continuous control tasks, where Q_v is not available. However, in these tasks, the adversary Adv only decreases the critic's evaluation of state s when taking an action a . Even if Adv did decrease the value of $V_{adv}(s)$, it does not necessarily lead to v choosing a sub-optimal action over the optimal one. Therefore, attacks that only rely on the value function require $\epsilon \geq 0.2$ to fool DRL policies effectively. For a more efficient attack, adversaries can clone v 's policy π_v into a proxy agent as π_{adv} , and try to maximize the total variation distance [39] in π_{adv} for states perturbed by universal perturbations. However, UAP-S, UAP-O and OSFW(U) need to be modified to compute the total variation distance, and we leave this as a future work.

Table 3 presents the online and offline computational cost for perturbation generation in continuous control tasks. Results are comparable with Table 1, and confirm that UAP-S, UAP-O and OSFW(U) can be mounted in real-time, while FGSM and OSFW cannot, since they have a higher online cost than v 's response time in continuous control.

5 DETECTION AND MITIGATION OF ADVERSARIAL PERTURBATIONS

A defender's goal is the opposite of the adversary Adv 's goal. Section 3.1 outlines three criteria for a successful attack. A good defense mechanism should thwart one or more of these criteria. We begin by surveying previously proposed defenses (Section 5.1), followed by an evaluation of the effectiveness of two of the most relevant defenses (Section 5.2) that aim to address the first (lowering the victim v 's return) and third attack criterion (evasion of detection). We then present a new approach to detect the presence of adversarial perturbations in state observations (Section 5.3.1), aimed at thwarting third attack criterion on evading defenses.

5.1 Defenses against Adversarial Examples

5.1.1 Defenses in image classification. Many prior studies proposed different methods to differentiate between normal images and adversarial examples. Meng and Chen [18] or Rouhani *et al.* [26] model the underlying data manifolds of the normal images to differentiate clean images from adversarial examples. Xu *et al.* [38] propose feature squeezing to detect adversarial examples. However, these detection methods are found to be inefficient [5] and not robust against adaptive adversaries that can specifically tailor adversarial perturbation generation methods for a given defense [34].

5.1.2 Defenses in DRL. Previous work [3, 14] has demonstrated that adversarial training improves agents' resilience to adversarial perturbations. However, Zhang *et al.* [39] show that adversarial training leads to performance degradation, and is not robust against strong attacks. In order to overcome the challenges of adversarial training, Zhang *et al.* [39] propose state-adversarial Markov decision process (SA-MDP). SA-MDP aims to find an optimal π under the strongest Adv using policy regularization. This regularization technique helps DRL agents *maintain* their performance even against adversarially perturbed inputs.

Visual Foresight [17] is a defense that is intended to *recover* the performance of a DRL agent in the presence of Adv . Visual Foresight deploys an action-conditioned frame prediction module to predict the current observation \hat{o}_t at time t using k previous observations $o_{t-k} : o_{t-1}$ and corresponding actions $a_{t-k} : a_{t-1}$. It also predicts the possible action \hat{a}_t for the partially predicted \hat{s} using $Q(\hat{s}, a)$, where $\hat{s} = \{f_{pre}(o_{t-N+1}), \dots, f_{pre}(\hat{o}_t)\}$. The difference between the action distribution (i.e., $\text{Softmax}(Q(s, a \in \mathcal{A}))$) obtained by the predicted \hat{s} and the current s is used to detect whether s is perturbed or not. In the case of detection, \hat{a}_t is selected to recover the performance of the agent. Both Visual Foresight and SA-MDP can recover the performance of agents when states are perturbed using prior attacks strategies in [11, 12, 35].

5.2 Effectiveness of Existing Defenses

While adversarial training [3, 14] presents promising results at defending against adversarial examples, it also leads to unstable training, performance degradation and is ineffective against strong attacks [39]. Moreover, Moosavi *et al.* [21] prove that despite a slight decrease in the fooling rate δ on the test set, Adv can easily compute another universal perturbation against retrained agents. Thus, directly applying adversarial retraining is not an effective defense against attacks using universal perturbations.

To investigate the limitations of previously proposed defenses for DRL, we implemented two defense methods that aims to retain the average return of v when it is under attack: Visual Foresight [17] and SA-MDP [39] (Section 5.1) both of which seek to prevent the first attack criterion that limits v to a low return. Visual Foresight also prevents the third attack criterion, and detects adversarial perturbations. Since we want to evaluate the effectiveness of Visual Foresight and SA-MDP, we focus on DQN agents for Pong and Freeway as these are the ones that are common between our experiments (Section 4) and these defenses ([17, 39]).

We implemented Visual Foresight from scratch for our DQN models following the original experimental setup in [17] by setting $k = 3$ to predict every 4th observation. We also set the pre-defined threshold value to 0.01, which is used for detecting adversarial perturbations, in order to achieve the highest detection rate and performance recovery. We downloaded state adversarial DQN agents, which are trained using SA-MDP, from their reference implementation³. SA-MDP agents only use one observation per s ; therefore, UAP-S would reduce to UAP-O for SA-MDP in this setup. Table 4 shows the average return for each agent under a different attack, and while equipped with different defenses. In Section 4, we established that when the perturbation bound ϵ is 0.01, all attacks are devastatingly effective. In the interest of evaluating the robustness of the defense, we also consider two higher ϵ values, 0.02 and 0.05.

Visual Foresight is an effective defense against FGSM and UAP-S as it can recover v 's average return. However, it is not very effective against OSFW, OSFW(U), and UAP-O. SA-MDP is better than Visual Foresight against OSFW and OSFW(U) when $\epsilon = 0.01$, but it fails to defend any attack in the case of Pong when $\epsilon \geq 0.02$. Notably, Visual Foresight's detection performance depends on the accuracy of the action-conditioned frame prediction module [17], and the pre-defined threshold value used for detecting adversarial perturbations.

³https://github.com/chenhongge/SA_DQN

		Average return \pm std in the presence of adversarial perturbation attacks					
ϵ	Defense	No attack	FGSM	OSFW	UAP-S	UAP-O	OSFW(U)
0.01	No defense	21.0 \pm 0.0	-21.0 \pm 0.0	-20.0 \pm 3.0	-21.0 \pm 0.0	-19.8 \pm 0.4	-21.0 \pm 0.0
	Visual Foresight [17]	21.0 \pm 0.0	21.0 \pm 0.0	-19.7 \pm 0.5	0.7 \pm 1.7	0.4 \pm 2.7	-21.0 \pm 0.0
	SA-MDP [39]	21.0 \pm 0.0	21.0 \pm 0.0	21.0 \pm 0.0	21.0 \pm 0.0	21.0 \pm 0.0	21.0 \pm 0.0
0.02	No defense	21.0 \pm 0.0	-19.9 \pm 1.3	-21.0 \pm 0.0	-20.8 \pm 0.6	-20.0 \pm 0.0	-21.0 \pm 0.0
	Visual Foresight [17]	21.0 \pm 0.0	21 \pm 0.0	-19.7 \pm 0.6	9.4 \pm 0.8	5.3 \pm 3.9	-20.5 \pm 0.5
	SA-MDP [39]	21.0 \pm 0.0	-14.6 \pm 8.8	-20.5 \pm 0.5	-20.6 \pm 0.5	-20.6 \pm 0.5	-21.0 \pm 0.0
0.05	No defense	21.0 \pm 0.0	-20.5 \pm 0.7	-21.0 \pm 0.0	-20.6 \pm 0.8	-20.0 \pm 0.0	-21.0 \pm 0.0
	Visual Foresight [17]	21.0 \pm 0.0	21.0 \pm 0.0	-20.0 \pm 0.0	7.6 \pm 4.7	-14.1 \pm 1.1	-21.0 \pm 0.0
	SA-MDP [39]	21.0 \pm 0.0	-21.0 \pm 0.0	-21.0 \pm 0.0	-20.6 \pm 0.5	-20.6 \pm 0.5	-21.0 \pm 0.0

(a) DQN agent playing Pong

		Average return \pm std in the presence of adversarial perturbation attacks					
ϵ	Defense	No attack	FGSM	OSFW	UAP-S	UAP-O	OSFW(U)
0.01	No defense	34.0 \pm 0.0	0.0 \pm 0.0	2.0 \pm 1.1	2.1 \pm 0.8	4.0 \pm 0.6	0.5 \pm 0.5
	Visual Foresight [17]	32.0 \pm 1.5	32.6 \pm 1.7	24.1 \pm 1.0	22.9 \pm 0.9	25.8 \pm 1.1	20.9 \pm 1.2
	SA-MDP [39]	30.0 \pm 0.0	30.0 \pm 0.0	30.0 \pm 0.0	30.0 \pm 0.0	30.0 \pm 0.0	30.0 \pm 0.0
0.02	No defense	34.0 \pm 0.0	0.0 \pm 0.0	1.0 \pm 0.0	0.1 \pm 0.3	0.8 \pm 0.6	0.0 \pm 0.0
	Visual Foresight [17]	32.0 \pm 1.5	32.6 \pm 1.7	1.1 \pm 0.3	24.0 \pm 2.0	25.6 \pm 1.0	4.4 \pm 1.1
	SA-MDP [39]	30.0 \pm 0.0	29.8 \pm 0.6	29.9 \pm 0.3	29.4 \pm 1.2	29.4 \pm 1.2	30.0 \pm 0.0
0.05	No defense	34.0 \pm 0.0	0.0 \pm 0.0	1.2 \pm 0.0	2.2 \pm 1.7	2.2 \pm 1.4	0.0 \pm 0.0
	Visual Foresight [17]	32.0 \pm 1.4	32.6 \pm 1.6	1.0 \pm 0.0	29.0 \pm 1.1	23.9 \pm 0.3	0.0 \pm 0.0
	SA-MDP [39]	30.0 \pm 0.0	21.1 \pm 1.3	20.9 \pm 0.8	21.1 \pm 1.7	21.1 \pm 1.7	21.1 \pm 1.7

(b) DQN agent playing Freeway

Table 4: Average returns (10 episodes) in the presence of different adversarial perturbation attacks, and equipped with different types of defenses. In each row, the best attack (lowest return) is in bold font. In each column, for a given ϵ value, the most robust (highest return) defense for that particular adversarial perturbation attack is shaded (green).

SA-MDP is able to partially retain the performance of v when $\epsilon = 0.01$ and 0.02 in the case of Freeway. Notably, v 's average return when it is under attack is still impacted, and SA-MDP cannot retain the same average return as when there is no attack. Furthermore, SA-MDP's effectiveness decreases drastically when the perturbation bound ϵ is increased to 0.05.

5.3 Detecting Adversarial Perturbations

The third criterion for a successful attack is evading detection (Section 3.1). For tasks with discrete action spaces, we now consider a defense that works in opposition to this criterion.

5.3.1 Action Distribution Divergence Detector(AD³). In a typical DRL episode, the sequential actions exhibit some degree of *temporal coherence*: the likelihood of the agent selecting a specific current action given a specific last action is consistent across different episodes. We also observed the temporal coherence is disrupted when the episode is subjected to an attack. We leverage this knowledge to propose a detection method, Action Distribution Divergence Detector (AD³), that calculates the statistical distance between the *conditional action probability distribution* (CAPD) of the current episode to the learned CAPD in order to detect whether the agent is under attack. Unlike prior work on detecting adversarial examples in the image domain [18, 26, 38], AD³ does not analyze the input image or tries to detect adversarial examples. Instead, it observes

the distribution of the actions triggered by the inputs and detects unusual action sequences.

To train AD³, v first runs k_1 episodes in a safe, controlled environment before the deployment. AD³ saves all actions taken during that time and approximates the conditional probability of the next action given the current one using the bi-gram model. We call the conditional probability of actions approximated by k_1 episodes as the *learned CAPD*. Second, to differentiate between the CAPD of a normal game versus a game that is under attack with high confidence, v runs another k_2 episodes in a safe environment. AD³ decides a threshold value th , where the statistical distance between the CAPD of the normal game and the learned CAPD falls mostly under this threshold. We use Kullback–Leibler (KL) divergence [15] as the statistical distance measure. The KL divergence between the learned CAPD and the CAPD of the current episode is calculated at each time-step starting after the first t_1 steps. We skip the first t_1 time-steps because the CAPD of the current episode is initially unstable and KL divergence is naturally high at the beginning of every episode. We set the threshold th as the p^{th} percentile of all KL-divergence values calculated for k_2 episodes. During deployment, AD³ continuously updates the CAPD of the current episode, and after t_1 time-steps, it calculates the KL-divergence between the CAPD of the current episode and the learned CAPD. If the KL-divergence exceeds the threshold th by $r\%$ or more during a

time window t_2 , then AD^3 raises an alarm that the agent is under attack.

We evaluate the precision and recall of AD^3 in three tasks with discrete action spaces (Pong, Freeway, and Breakout) against all proposed attacks. AD^3 can detect all five attacks in Pong with perfect precision and recall scores in all configurations. In Freeway, AD^3 has a perfect precision and recall scores for 12 out of 15 different setups (FGSM against DQN agent, OSFW against PPO agent, and OSFW against PPO agent). AD^3 is less effective against Breakout as this task often terminates too quickly when it is under an attack. Detailed discussion on the performance of AD^3 and the full result of the evaluation can be found in Appendix C.

Visual Foresight aims to detect adversarial perturbations for each s in an episode. This means that Visual Foresight can raise many false alarms in episodes with no attack because it cannot differentiate clean states from adversarially perturbed states when using a low pre-defined threshold value. On the other hand, AD^3 does not detect the presence of Adv at every s but instead AD^3 takes information from multiple actions within an episode and makes a judgement regarding the presence of Adv . Therefore, it is difficult to compare AD^3 and Visual Foresight directly, as these methods are optimized for different purposes.

AD^3 is designed for attacks where adversaries apply their adversarial perturbations consistently throughout the episode. As such, Adv with the knowledge of the detection strategy could apply their adversarial perturbation at a lower frequency to avoid detection. However, lowering the attack frequency also decreases the attack effectiveness. Another way for Adv to evade AD^3 is to perform targeted attacks to lure v into a specific state, where the adversarial perturbation is applied to a limited number of states in an episode. This attack type is out of the scope of our paper, and defense strategies against it will be explored in future work.

5.3.2 Adversary vs. defender strategy with negative returns. In any DRL task where there is a clear negative result for an episode (e.g., losing a game) or the possibility of negative return, a reasonable choice for v is to suspend an episode when Adv 's presence is detected. For example, in Pong, a negative result would be when the computer (as the opponent) reaches the score of 21 before v does. Suspending an episode prevents v from losing the game. Defense mechanisms such as Visual Foresight and SA-MDP are useful in retaining or recovering v 's return; however, they may not always prevent v from falling into a negative result, e.g., losing the game in Pong. Combining a recovery/retention mechanism with suspension on attack detection can reduce the number of losses for v .

To illustrate the effectiveness of combining a detection mechanism like AD^3 with a retention/recovery mechanism, we designed an experiment using a DQN agent playing Pong to compare the *losing rate* of v when it is under attack. We only use Pong for this experiment as Pong has a clear negative result. In this setting, an episode ends with the loss when (a) the computer reaches 21 points before v , or (b) AD^3 did not raise an alarm. The result of this experiment can be found in Table 5. As shown in this table, Visual Foresight is not effective in reducing the losing rate of v for OSFW and OSFW(U) for all ϵ . SA-MDP is effective in avoiding losses when $\epsilon = 0.01$, however it fails against all universal perturbations when

ϵ	Method	No attack	Losing Rate				
			FGSM	OSFW	UAP-S	UAP-O	OSFW(U)
0.01	No defense	0.0	1.0	1.0	1.0	1.0	1.0
	Visual Foresight [17]	0.0	0.0	1.0	0.0	0.2	1.0
	SA-MDP [39]	0.0	0.0	0.0	0.0	0.0	0.0
	AD^3	0.0	0.0	0.0	0.0	0.0	0.0
0.02	No defense	0.0	1.0	1.0	1.0	1.0	1.0
	Visual Foresight [17]	0.0	0.0	1.0	0.0	0.3	1.0
	SA-MDP [39]	0.0	0.9	1.0	1.0	1.0	1.0
	AD^3	0.0	0.0	0.0	0.0	0.0	0.0

Table 5: Losing rate (10 episodes) of DQN agents playing Pong with or without additional defense or detection method. Losing rate is calculated by counting the number of games where the computer arrives at 21 points first in an episode. If AD^3 raises an alarm before an episode ends, then v does not lose the game. In each row, the best attack (highest losing rate) is in bold font. In each row, for a given ϵ value, the least robust (highest losing rate) defense for that particular adversarial perturbation attack is shaded (red).

$\epsilon = 0.02$. In contrast, AD^3 can detect the presence of adversarial perturbations in all games.

Although retention/recovery and detection are two orthogonal aspects of defense, our results above suggest that they can be combined in tasks with negative returns or results in order to more effectively thwart Adv from achieving its first goal.

6 CONCLUSION

We showed that white-box universal perturbation attacks are effective in fooling DRL policies in real-time. Our evaluation of the three different attacks (UAP-S, UAP-O and OSFW(U)) demonstrates that universal perturbations are effective in tasks with discrete action spaces. Universal perturbation attacks are also able to generalize to continuous control tasks with the same efficiency. We confirmed that the effectiveness of prior defenses depends on the perturbation bound, and fail to completely recover the agent performance when they are confronted with universal perturbations of larger bounds. We proposed a detection mechanism, AD^3 , that detects all five attacks evaluated in the paper. AD^3 can be combined with other defense techniques to protect agents in tasks with negative returns or results to stop the adversary from achieving its goal. In the future, we plan to extend our attacks to the black-box case by first mounting a model extraction attack and then applying our current techniques to find transferable universal perturbations.

REFERENCES

- [1] Shumeet Baluja and Ian Fischer. 2018. Learning to Attack: Adversarial Transformation Networks. In *Proceedings of AAAI-2018*. <http://www.esprockets.com/papers/aaai2018.pdf>
- [2] Vahid Behzadan and Arslan Munir. 2017. Vulnerability of deep reinforcement learning to policy induction attacks. In *International Conference on Machine Learning and Data Mining in Pattern Recognition*. Springer, 262–275.
- [3] Vahid Behzadan and Arslan Munir. 2017. Whatever does not kill deep reinforcement learning, makes it stronger. *arXiv preprint arXiv:1712.09344* (2017).
- [4] Marc G Bellemare, Yavar Naddaf, Joel Veness, and Michael Bowling. 2013. The arcade learning environment: An evaluation platform for general agents. *Journal of Artificial Intelligence Research* 47 (2013), 253–279.
- [5] Nicholas Carlini and David Wagner. 2017. Adversarial examples are not easily detected: Bypassing ten detection methods. In *Proceedings of the 10th ACM workshop on artificial intelligence and security*. 3–14.
- [6] Nicholas Carlini and David Wagner. 2017. Towards Evaluating the Robustness of Neural Networks. In *2017 IEEE Symposium on Security and Privacy (SP)*. 39–57.

https://doi.org/10.1109/SP.2017.94

[7] Kenneth T Co, Luis Muñoz-González, Sixte de Maupéou, and Emil C Lupu. 2019. Procedural noise adversarial examples for black-box attacks on deep convolutional networks. In *Proceedings of the 2019 ACM SIGSAC conference on computer and communications security*. 275–289.

[8] Adam Gleave, Michael Dennis, Neel Kant, Cody Wild, Sergey Levine, and Stuart Russell. 2019. Adversarial policies: Attacking deep reinforcement learning. *arXiv preprint arXiv:1905.10615* (2019).

[9] Ian Goodfellow, Jonathon Shlens, and Christian Szegedy. 2015. Explaining and Harnessing Adversarial Examples. In *International Conference on Learning Representations*. http://arxiv.org/abs/1412.6572

[10] Jamie Hayes and George Danezis. 2018. Learning universal adversarial perturbations with generative models. In *2018 IEEE Security and Privacy Workshops (SPW)*. IEEE, 43–49.

[11] Sandy Huang, Nicolas Papernot, Ian Goodfellow, Yan Duan, and Pieter Abbeel. 2017. Adversarial Attacks on Neural Network Policies. *arXiv* (2017). https://arxiv.org/abs/1702.02284

[12] Leonard Hussenot, Matthieu Geist, and Olivier Pietquin. 2020. CopyCAT: Taking Control of Neural Policies with Constant Attacks. In *International Conference on Autonomous Agents and Multi-Agent Systems (AAMAS)*. https://arxiv.org/abs/1905.12282

[13] Matthew Inkawich, Yiran Chen, and Hai Li. 2020. Snooping Attacks on Deep Reinforcement Learning. In *Proceedings of the 19th International Conference on Autonomous Agents and MultiAgent Systems* (Auckland, New Zealand) (AAMAS '20). Richland, SC, 557–565.

[14] Jernej Kos and Dawn Song. 2017. Delving into adversarial attacks on deep policies. In *5th International Conference on Learning Representations, ICLR 2017, Toulon, France, April 24-26, 2017, Workshop Track Proceedings*. OpenReview.net. https://openreview.net/forum?id=Bjcb5mFe

[15] Solomon Kullback and Richard A Leibler. 1951. On information and sufficiency. *The annals of mathematical statistics* 22, 1 (1951), 79–86.

[16] Yen-Chen Lin, Zhang-Wei Hong, Yuan-Hong Liao, Meng-Li Shih, Ming-Yu Liu, and Min Sun. 2017. Tactics of Adversarial Attack on Deep Reinforcement Learning Agents. In *Proceedings of the Twenty-Sixth International Joint Conference on Artificial Intelligence, IJCAI 2017, Melbourne, Australia, August 19-25, 2017*. ijcai.org, 3756–3762. https://doi.org/10.24963/ijcai.2017/525

[17] Yen-Chen Lin, Ming-Yu Liu, Min Sun, and Jia-Bin Huang. 2017. Detecting Adversarial Attacks on Neural Network Policies with Visual Foresight. *CoRR* abs/1710.00814 (2017). arXiv:1710.00814 http://arxiv.org/abs/1710.00814

[18] Dongyu Meng and Hao Chen. 2017. Magnet: a two-pronged defense against adversarial examples. In *Proceedings of the 2017 ACM SIGSAC Conference on Computer and Communications Security*. 135–147.

[19] Volodymyr Mnih, Adrià Puigdomènech Badia, Mehdi Mirza, Alex Graves, Timothy P. Lillicrap, Tim Harley, David Silver, and Koray Kavukcuoglu. 2016. Asynchronous Methods for Deep Reinforcement Learning. In *Proceedings of the 33nd International Conference on Machine Learning, ICML 2016, New York City, NY, USA, June 19-24, 2016*, Vol. 48. 1928–1937.

[20] Volodymyr Mnih, Koray Kavukcuoglu, David Silver, Andrei A. Rusu, Joel Veness, Marc G. Bellemare, Alex Graves, Martin A. Riedmiller, Andreas Fidjeland, Georg Ostrovski, Stig Petersen, Charles Beattie, Amir Sadik, Ioannis Antonoglou, Helen King, Dharshan Kumaran, Daan Wierstra, Shane Legg, and Demis Hassabis. 2015. Human-level control through deep reinforcement learning. *Nature* 518, 7540 (2015), 529–533. https://doi.org/10.1038/nature14236

[21] Seyed-Mohsen Moosavi-Dezfooli, Alhussein Fawzi, Omar Fawzi, and Pascal Frossard. 2017. Universal adversarial perturbations. In *Proceedings of the IEEE conference on computer vision and pattern recognition*. 1765–1773.

[22] Seyed-Mohsen Moosavi-Dezfooli, Alhussein Fawzi, and Pascal Frossard. 2016. Deepfool: a simple and accurate method to fool deep neural networks. In *Proceedings of the IEEE conference on computer vision and pattern recognition*. 2574–2582.

[23] Konda Reddy Mopuri, Utsav Garg, and R Venkatesh Babu. 2017. Fast feature fool: A data independent approach to universal adversarial perturbations. *arXiv preprint arXiv:1707.05572* (2017).

[24] Konda Reddy Mopuri, Utkarsh Ojha, Utsav Garg, and R Venkatesh Babu. 2018. NAG: Network for adversary generation. In *Proceedings of the IEEE Conference on Computer Vision and Pattern Recognition*. 742–751.

[25] Nicolas Papernot, Patrick McDaniel, Somesh Jha, Matt Fredrikson, Z Berkay Celik, and Ananthram Swami. 2016. The limitations of deep learning in adversarial settings. In *2016 IEEE European symposium on security and privacy (EuroS&P)*. IEEE, 372–387.

[26] Bita Darvish Rouhani, Mohammad Samragh, Mojtaba Javaheripi, Tara Javidi, and Farinaz Koushanfar. 2018. Deepfense: Online accelerated defense against adversarial deep learning. IEEE, 1–8.

[27] Olga Russakovsky, Jia Deng, Hao Su, Jonathan Krause, Sanjeev Satheesh, Sean Ma, Zhiheng Huang, Andrej Karpathy, Aditya Khosla, Michael Bernstein, et al. 2015. Imagenet large scale visual recognition challenge. *International journal of computer vision* 115, 3 (2015), 211–252.

[28] John Schulman, Filip Wolski, Prafulla Dhariwal, Alec Radford, and Oleg Klimov. 2017. Proximal Policy Optimization Algorithms. *CoRR* abs/1707.06347 (2017). arXiv:1707.06347 http://arxiv.org/abs/1707.06347

[29] Jianwen Sun, Tianwei Zhang, Xiaofei Xie, Lei Ma, Yan Zheng, Kangjie Chen, and Yang Liu. 2020. Stealthy and efficient adversarial attacks against deep reinforcement learning. In *Proceedings of the AAAI Conference on Artificial Intelligence*. AAAI Press, 5883–5891.

[30] Richard S Sutton and Andrew G Barto. 2018. *Reinforcement learning: An introduction*. MIT press.

[31] Christian Szegedy, Wojciech Zaremba, Ilya Sutskever, Joan Bruna, Dumitru Erhan, Ian Goodfellow, and Rob Fergus. 2014. Intriguing properties of neural networks. In *International Conference on Learning Representations*. http://arxiv.org/abs/1312.6199

[32] Yuval Tassa, Yotam Doron, Alistair Muldal, Tom Erez, Yazhe Li, Diego de Las Casas, David Budden, Abbas Abdolmaleki, Josh Merel, Andrew Lefrancq, et al. 2018. Deepmind control suite. *arXiv preprint arXiv:1801.00690* (2018).

[33] Emanuel Todorov, Tom Erez, and Yuval Tassa. 2012. Mujoco: A physics engine for model-based control. In *2012 IEEE/RSJ International Conference on Intelligent Robots and Systems*. IEEE, 5026–5033.

[34] Florian Tramer, Nicholas Carlini, Wieland Brendel, and Aleksander Madry. 2020. On Adaptive Attacks to Adversarial Example Defenses. In *Advances in Neural Information Processing Systems*, H. Larochelle, M. Ranzato, R. Hadsell, M. F. Balcan, and H. Lin (Eds.), Vol. 33. Curran Associates, Inc., 1633–1645.

[35] Edgar Tretschk, Seong Joon Oh, and Mario Fritz. 2018. Sequential Attacks on Agents for Long-Term Adversarial Goals. *CoRR* abs/1805.12487 (2018). arXiv:1805.12487 http://arxiv.org/abs/1805.12487

[36] Xian Wu, Wenbo Guo, Hua Wei, and Xinyu Xing. 2021. Adversarial Policy Training against Deep Reinforcement Learning. In *30th USENIX Security Symposium (USENIX Security 21)*. USENIX Association, 1883–1900. https://www.usenix.org/conference/usenixsecurity21/presentation/wu-xian

[37] Chaowei Xiao, Xinlei Pan, Warren He, Jian Peng, Mingjie Sun, Jinfeng Yi, Bo Li, and Dawn Song. 2019. Characterizing Attacks on Deep Reinforcement Learning. *arXiv preprint arXiv:1907.09470* (2019).

[38] Weilin Xu, David Evans, and Yanjun Qi. 2018. Feature Squeezing: Detecting Adversarial Examples in Deep Neural Networks. In *25th Annual Network and Distributed System Security Symposium, NDSS*. The Internet Society.

[39] Huan Zhang, Hongge Chen, Chaowei Xiao, Bo Li, Mingyan Liu, Duane Boning, and Cho-Jui Hsieh. 2020. Robust Deep Reinforcement Learning against Adversarial Perturbations on State Observations. In *Advances in Neural Information Processing Systems*, Vol. 33. Curran Associates, Inc., 21024–21037.

[40] Xiangyu Zhang, Jianhua Zou, Kaiming He, and Jian Sun. 2015. Accelerating very deep convolutional networks for classification and detection. *IEEE transactions on pattern analysis and machine intelligence* 38, 10 (2015), 1943–1955.

[41] Yiren Zhao, Ilia Shumailov, Han Cui, Xitong Gao, Robert Mullins, and Ross Anderson. 2020. Blackbox attacks on reinforcement learning agents using approximated temporal information. In *2020 50th Annual IEEE/IFIP International Conference on Dependable Systems and Networks Workshops (DSN-W)*. IEEE, IEEE Computer Society, Los Alamitos, CA, USA, 16–24.

A PROOF OF EQUATION 6

In this section, we provide a formal proof of Equation 6 that was used to find the perturbation in UAP-O.

In UAP-O, we defined an additional constraint for the perturbation as $\tilde{r}_j = \tilde{r}_k$, $\forall j, k \in \{t - N + 1, \dots, t\}$, so that the same \tilde{r}_j is applied into all observations o_j . As pointed out in Section 3.2, at i -th iteration, the DeepFool algorithm computes the i -th perturbation \mathbf{r}_i for i -th state s_i as

$$\Delta \mathbf{r}_i \leftarrow \frac{|\mathcal{Q}'(s_i^*, a_i^*)|}{\|\mathbf{w}'_i\|_2^2} \mathbf{w}'_i. \quad (8)$$

We can keep the term $|\mathcal{Q}'(s_i^*, a_i^*)|/\|\mathbf{w}'_i\|_2^2$ as constant, since it gives the magnitude of the perturbation update $\Delta \mathbf{r}_i$, and we can maintain the same magnitude of $\Delta \mathbf{r}_i$ in $\tilde{\Delta \mathbf{r}}_i$. Then, in UAP-O, DeepFool finds the closest $\tilde{\Delta \mathbf{r}}_i$ to $\Delta \mathbf{r}_i$ by minimizing the direction of the perturbation as $\|\mathbf{w}'_i - \tilde{\Delta \mathbf{r}}_i\|_2^2$.

We can find the optimal $\tilde{\Delta \mathbf{r}}_i$ by setting $\partial \|\mathbf{w}'_i - \tilde{\Delta \mathbf{r}}_i\|_2^2 / \partial \tilde{\Delta \mathbf{r}}_i$ to zero for all $j \in \{t - N + 1, \dots, t\}$, where N denotes the total number of observations inside state s . We also set all $\tilde{\Delta \mathbf{r}}_{i,j}$ into the same variable $\tilde{r}_{i,t}$. Therefore, we simply obtain $\tilde{\Delta \mathbf{r}}_{i,t}$ by finding the point

where the partial derivative is equal to zero as in Equation 9.

$$\begin{aligned} \frac{\partial \|\mathbf{w}'_{\hat{l}} - \Delta \tilde{r}_{i_t}\|_2}{\partial \Delta \tilde{r}_{i_t}} &= \frac{\partial((\mathbf{w}'_{\hat{l}_t} - \Delta \tilde{r}_{i_t})^2 + \dots + (\mathbf{w}'_{\hat{l}_{t-N}} - \Delta \tilde{r}_{i_t})^2)^{1/2}}{\partial \Delta \tilde{r}_{i_t}} \\ 0 &= \frac{\partial f(\Delta \tilde{r}_{i_t})^{1/2}}{\partial \Delta \tilde{r}_{i_t}} \\ 0 &= 0.5f(\Delta \tilde{r}_{i_t})^{-3/2} \left(2(N+1)\Delta \tilde{r}_{i_t} - 2 \sum_{k=t-N+1}^t \mathbf{w}'_{\hat{l}_k} \right) \end{aligned} \quad (9)$$

The squared difference function $f(\Delta \tilde{r}_{i_t})^{-3/2} \geq 0$, and only equal to zero when $\Delta \tilde{r}_{i_t} = 0$, which does not give any useful perturbation. Therefore, Equation 9 is solved when $\mathbf{w}'_{\hat{l}_k} = \Delta \tilde{r}_{i_t}, \forall k \in \{t-N+1, \dots, t\}$. Therefore, by putting back the constant, DeepFool computes the perturbation at i^{th} iteration as

$$\Delta \tilde{r}_{i_j} \leftarrow \frac{|Q'(\mathbf{s}_i^*, a_{\hat{l}})|}{N \|\mathbf{w}'_{\hat{l}}\|_2^2} \sum_{k=(t-N+1)}^t \mathbf{w}'_{\hat{l}_k}. \quad (10)$$

B ADVERSARIAL PERTURBATIONS

On top of comparing the perturbation size in Pong (Figure 3, Section 4.2), we also include results comparing the perturbation size for other games. As shown in Figure 5, FGSM generates a perturbation that contains grey patches where the sign of the gradient of the loss is zero against the DQN agent. It has also completely black and white pixels due to the l_∞ constraint, which makes the perturbation more visible. In addition, Figure 6 compares the clean and perturbed frames generated by different attacks. Note that we inject the perturbation into pre-processed frames (i.e., resized and gray-scale frames), so we show both RGB and gray-scale clean frames in Figure 5 and Figure 6. In Pong, the perturbation size in UAP-S is the smallest when compared to other attacks.

C OPTIMAL PARAMETERS FOR AD³

We performed a grid search to find optimal parameters for AD³ in Breakout, Pong, and Freeway using three different agents (DQN, A2C, and PPO) and choose the parameters with the best F1-score. The optimal parameter values can be found in Table 2. The precision and recall scores of AD³ against five different attacks at $\epsilon = 0.01$ can also be found in this table. AD³ is able to detect the presence of the adversary Adv with perfect precision and recall for most environments and agents. However, there are some combinations of environment and agent, where AD³ has a low recall and/or precision.

Attacks such as OSFW(U) in Freeway against PPO agents have a low action change rate (as low as 20% – 30% in some episodes), and the resulting average return is still high. This means that Adv does not change many actions in an episode. This low action change rate is consistent with all of the combinations of the game, agent, and attack that have a low recall score. As AD³ relies on modeling the distribution of the victim v 's action distribution during an episode, it cannot detect the presence of Adv if there are not enough actions influenced by the attack in an episode. This means that a low action change rate from Adv would make it difficult for AD³ to detect. The precision of AD³ in Breakout is lower than other environments, since episodes in Breakout terminate very quickly (as fast as in

Game	Agent	Parameters	Attack	Precision/Recall
Pong	dqn	$k_1 = 12, k_2 = 24,$ $p = 100,$ $r = 0.9,$ $t_1 = 400,$ $t_2 = 200$	FGSM	1.0/1.0
			OSFW(U)	1.0/1.0
			UAP-S	1.0/1.0
			UAP-O	1.0/1.0
			OSFW	1.0/1.0
	a2c	$k_1 = 12, k_2 = 24,$ $p = 100,$ $r = 0.9,$ $t_1 = 400,$ $t_2 = 200$	FGSM	1.0/1.0
			OSFW	1.0/1.0
			UAP-S	1.0/1.0
			UAP-O	1.0/1.0
	ppo	$k_1 = 12, k_2 = 24,$ $p = 100,$ $r = 0.9,$ $t_1 = 400,$ $t_2 = 200$	FGSM	1.0/1.0
			OSFW	1.0/1.0
			UAP-S	1.0/1.0
			UAP-O	1.0/1.0
Freeway	dqn	$k_1 = 12, k_2 = 24,$ $p = 95,$ $r = 0.8,$ $t_1 = 400,$ $t_2 = 200$	FGSM	1.0/0.8
			OSFW	1.0/1.0
			UAP-S	1.0/1.0
			UAP-O	1.0/1.0
			OSFW(U)	1.0/1.0
	a2c	$k_1 = 12, k_2 = 24,$ $p = 100,$ $r = 1.0,$ $t_1 = 400,$ $t_2 = 200$	FGSM	1.0/1.0
			OSFW	1.0/1.0
			UAP-S	1.0/1.0
			UAP-O	1.0/1.0
	ppo	$k_1 = 12, k_2 = 24,$ $p = 90,$ $r = 0.9,$ $t_1 = 200,$ $t_2 = 200$	FGSM	1.0/1.0
			OSFW	1.0/0.5
			UAP-S	1.0/1.0
			UAP-O	1.0/1.0
Breakout	dqn	$k_1 = 12, k_2 = 24,$ $p = 97,$ $r = 0.6,$ $t_1 = 60,$ $t_2 = 40$	FGSM	0.7/1.0
			OSFW	0.7/1.0
			UAP-S	0.7/1.0
			UAP-O	0.7/1.0
			OSFW(U)	0.2/0.2
	a2c	$k_1 = 12, k_2 = 24,$ $p = 100,$ $r = 0.8,$ $t_1 = 60,$ $t_2 = 40$	FGSM	1.0/1.0
			OSFW	1.0/1.0
			UAP-S	1.0/0.8
			UAP-O	1.0/1.0
	ppo	$k_1 = 12, k_2 = 24,$ $p = 97,$ $r = 0.8,$ $t_1 = 60,$ $t_2 = 40$	FGSM	1.0/1.0
			OSFW	0.8/1.0
			UAP-S	0.8/1.0
			UAP-O	0.8/1.0
			OSFW(U)	0.8/1.0

Table 6: Optimal values of AD³ to detect five different attacks: FGSM, OSFW, UAP-S, UAP-O, and OSFW(U) at $\epsilon = 0.01$ for all games and agents over ten episodes.

112 time steps) when v is under attack. This means that to detect the presence of Adv , AD³ has to raise an alarm early in Breakout. However, AD³ relies on modelling CAPD of the current episode, and it takes time to converge. Before CAPD converges, the anomaly score is going to be high for any episode, including episodes with no attack presence. As an episode can terminate quickly in Breakout, AD³ cannot store enough actions for CAPD to converge, and this is reflected in the reported low precision values. In OSFW(U) against PPO agent in Breakout, both the precision and recall scores are low, since the action change rate of OSFW(U) in an episode is around

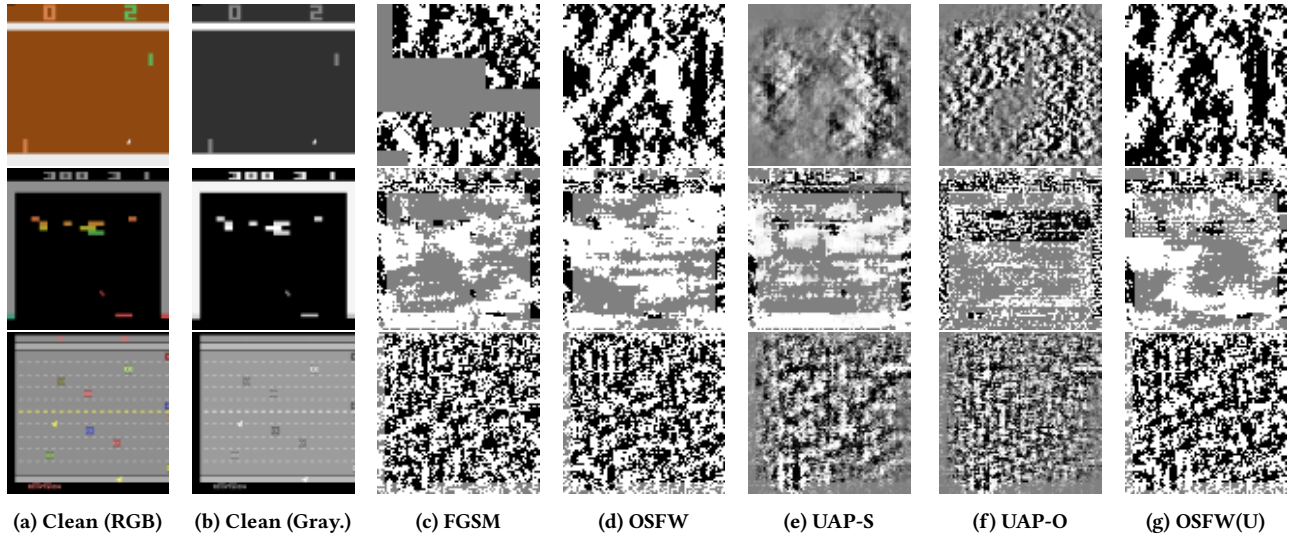


Figure 5: Comparison of perturbation size added into the same clean (in both RGB and gray-scale) observation in different attacks when $\epsilon = 0.01$. UAP-S and UAP-O generate smaller perturbations. Top row: DQN agent playing Pong, Middle row: PPO agent playing Breakout, Bottom row: A2C agent playing Freeway. In perturbation images, black pixels: -0.01 , white pixels: $+0.01$, gray pixels: 0.0 .

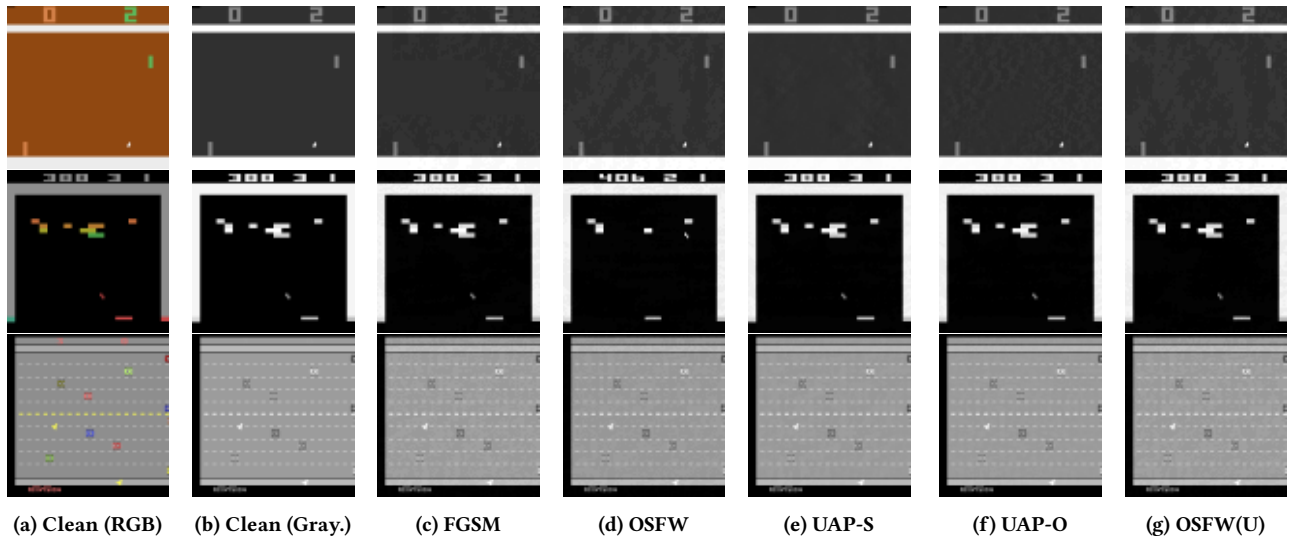


Figure 6: Comparison of the clean (in both RGB and gray-scale) and perturbed observations in different attacks when $\epsilon = 0.01$. UAP-S and UAP-O generate smaller perturbations that are less visible. Top row: DQN agent playing Pong, Middle row: PPO agent playing Breakout, Bottom row: A2C agent playing Freeway.

20% - 30% (but still an effective attack), and CAPD is not given a sufficient amount of time to converge.